Exchange frequencies in two-dimensional solids

2002 J. Phys.: Condens. Matter 14 9099

(http://iopscience.iop.org/0953-8984/14/40/304)

INSTITUTE OF PHYSICS PUBLISHING JOURNAL OF PHYSICS: CONDENSED MATTER

J. Phys.: Condens. Matter **14** (2002) 9099–9107 PII: S0953-8984(02)36510-X

Exchange frequencies in two-dimensional solids

B Bernu[1] **and D M Ceperley**[2]

[1] Laboratoire de Physique Théorique des Liquides, UMR 7600 of CNRS, Université P et M Curie, boite 121, 4 Place Jussieu, 75252 Paris, France
[2] Department of Physics and NCSA, University of Illinois, Urbana-Champaign, Urbana, IL 61801, USA

E-mail: bernu@lptl.jussieu.fr and ceperley@uiuc.edu

Received 2 May 2002, in final form 12 June 2002
Published 27 September 2002
Online at stacks.iop.org/JPhysCM/14/9099

Abstract

In quantum solids composed of fermion particles, such as helium-3 and electrons, the low-temperature physics is governed by spin exchanges, according to the Thouless theory. We present path integral Monte Carlo calculations of ring exchange energies on 'clean' two-dimensional crystals of both helium-3 and electrons. We see a remarkable similarity of the results for these two 'opposite' systems. They are both ferromagnetic in the semi-classical limit (strong coupling) and antiferromagnetic near the melting transition where the relative exchange energies become equivalent. We focus here on the importance of long-ring exchanges near the melting transition. The total energy associated to exchanges may diverge, leading to a possible mechanism for the melting transition.

(Some figures in this article are in colour only in the electronic version)

1. Introduction

In spinless solids, the low-temperature physics is governed by the low excitations, the phonons. They provide a specific heat of $(T/\theta_D)^2$ in two dimensions, where the Debye temperature θ_D measures the typical kinetic energy of a particle in its local potential (see figure 1 for $T > 0.3$ K). Despite their 'opposite' types of interaction, short-range and hard-core-like for helium versus long-range and 'smooth-core'-like for electrons, these systems have some similarities: two-dimensional helium-3 and electrons solidify on a triangular lattice. Because of the 'opposite' nature of their potentials, the solid is found at high density for helium and low density for electrons, i.e. in the strong-coupling or semi-classical limit. Also, electrons and helium-3 are fermions with spin-$\frac{1}{2}$ (on the nuclei for helium-3, whereas its two electrons are in a total spin-0 state).

When $T/\theta_D \ll 1$, the spatial degrees of freedom are frozen. But helium atoms, like electrons, have a large zero-point motion. They eventually exchange their position, resulting

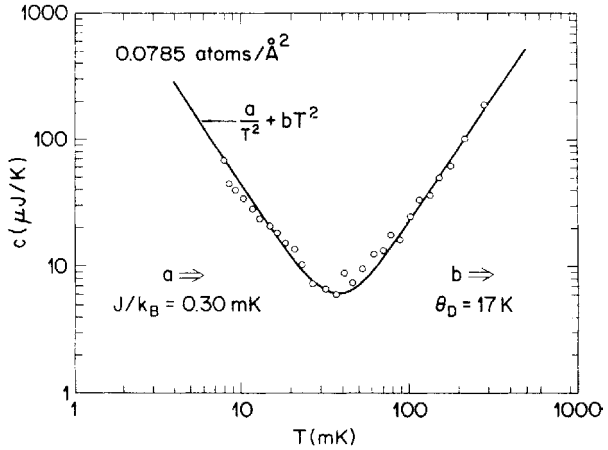

Figure 1. The specific heat measured by Greywall for 2D helium-3 adsorbed on graphite [1]. One can see clearly the crossover between the spin contribution in $1/T^2$ and the phonon contribution in T^2.

in a spin exchange that will modify the thermodynamics because of antisymmetry [1, 2]. The simplest effective model describing spin exchanges is the Heisenberg model:

$$H_{\text{spin}} = \sum_{\langle i,j \rangle} J P_{ij} = \sum_{\langle i,j \rangle} (2J \boldsymbol{S}_i \cdot \boldsymbol{S}_j - \tfrac{1}{2}). \tag{1}$$

where J is the energy associated with the spin permutation P, and the last equality holds for spin-$\frac{1}{2}$. Assuming that $J \ll \theta_D$, we look at the leading contribution of H_{spin} to the specific heat at high temperatures (meaning $J \ll T \ll \theta_D$) which behaves as $(J/T)^2$ (see figure 1 now for $T < 0.3$ K). For $T \gg J$, the spins are free and no longer contribute to the specific heat and the particles can be distinguishable.

There is a clear difference in energy scale of at least three orders of magnitude between the degrees of freedom associated with the spins and those associated with the spatial coordinates. The simple Heisenberg Hamiltonian does not reproduce experimental data on the specific heat or the magnetic susceptibility except in the strong-coupling limit [1]. Thus the model of a multi-spin exchange (MSE) Hamiltonian has been proposed to describe the physics of the spins at low temperature [2, 7]. In the next section, we present a short description of the Thouless theory and how we evaluate the coupling constants of the effective Hamiltonian from path integral Monte Carlo (PIMC) simulations. In section 3 we will present some results and the corresponding magnetic phase diagram. In the section 4, we analyse the data near the melting transition. We focus especially on the convergence of the MSE model with respect to the cycle length n. Indeed, if the coupling constants are believed to decrease exponentially with n, the number of cycles of length n also increases exponentially.

2. The effective Hamiltonian

To determine the low-temperature wavefunction of the spins, we assume that the Thouless theory can be applied [3]. In this approach, we first consider the spinless Hamiltonian in spatial coordinates. At low temperature, each particle oscillates with a zero-point motion around a lattice position Z. Eventually, during these random motions, a tunnelling process occurs, resulting in a permutation of some particles. Because the energy scale is so different

($J \ll \theta_D$), such an event is sufficiently rare that it can be studied independently of other such events. Thus, we are left with a two-well problem in a multi-dimensional space. In this two-well system the ground state ψ_0 of energy E_0 is symmetrical and the first excited state ψ_1 of energy E_1 is antisymmetrical. Other states have much higher energies and can be neglected. The diagonal density matrix element $\langle Z|\exp(-\beta H)|Z\rangle$ and the off-diagonal density matrix element $\langle Z|\exp(-\beta H)|PZ\rangle$ can be expanded as

$$\langle Z|\exp(-\beta H)|Z\rangle = \psi_0^2(Z)\mathrm{e}^{-\beta E_0} + \psi_1^2(Z)\mathrm{e}^{-\beta E_1} + \cdots$$
$$\langle Z|\exp(-\beta H)|PZ\rangle = \psi_0^2(Z)\mathrm{e}^{-\beta E_0} - \psi_1^2(Z)\mathrm{e}^{-\beta E_1} + \cdots$$

where we have used the symmetry properties of the first two states. The ratio of these two density matrix elements is then [6]:

$$F_P(\beta) = \frac{\langle Z|\exp(-\beta H)|PZ\rangle}{\langle Z|\exp(-\beta H)|Z\rangle} = \tanh(J_P(\beta - \beta_0)), \tag{2}$$

where $J_P = (E_1 - E_0)/2$ is the exchange frequency and $\beta_0 = \ln|\psi_1(Z)/\psi_0(Z)|$. The evaluation of $F_P(\beta)$ leads to the exchange energy J_P.

Using the mapping of a quantum system to a classical system of 'polymers', one can reinterpret $F_P(\beta)$ as the free energy necessary to make an exchange beginning with one arrangement of particles to lattice sites Z and ending on a permuted arrangement PZ. To evaluate $F_P(\beta)$, we use the optimized method introduced by Bennett [4] to calculate free energy differences of two chemical species A and B. Here A is the non-permuting system and B the permuting one. The idea is to try to transform A into B and to calculate the probability of success. More details can be found in [5–8].

The Thouless theory [3] tells us that there is an effective MSE Hamiltonian describing the spin physics:

$$H_{\mathrm{MSE}} = -\sum_P (-1)^P J_P P \tag{3}$$

where J_P is the energy J_P associated with the permutation of the P particles. It is in finding the eigenfunctions of this Hamiltonian that the fermion problem is encountered. In the semi-classical limit, WKB calculations provide useful values of these exchange energies [9, 10], especially for the Wigner crystal [11].

Using PIMC, we have evaluated the ring exchange frequencies up to nine-body permutations. This method was successfully applied for the first time to bulk helium-3 in [6]

3. Results and magnetic phase diagram

The semi-classical (WKB) calculations, accurate in the strong-coupling limit, give exchange energies which for the Wigner crystal vary as [9, 11]

$$J_P = A_P b_P^{1/2} r_s^{-5/4} \mathrm{e}^{-b_P r_s^{1/2}}. \tag{4}$$

where $b_P r_s^{1/2}$ is the minimum value of the action integral along the exchanging path. Assuming that b_P is constant, we can put all quantum fluctuation effects in the prefactor A_P. Thus this formula tells us that the exchange energies vary exponentially with the density. This is indeed what we find both for helium 3 (see figure 2) and for electrons (see figure 3). Moreover, for the Wigner crystal, we find that A_P is always of the order of unity. But the relative values of the Js change from the WKB limit to the strong-fluctuation scenario near the melting transition.

Introducing the Js in the effective MSE Hamiltonian of equation (3), we now consider the character of the ground state. Limiting this analysis to the first important loop exchanges (two-, three-, four-, five- and hexagonal six-body exchange), the magnetic phase diagram is deduced

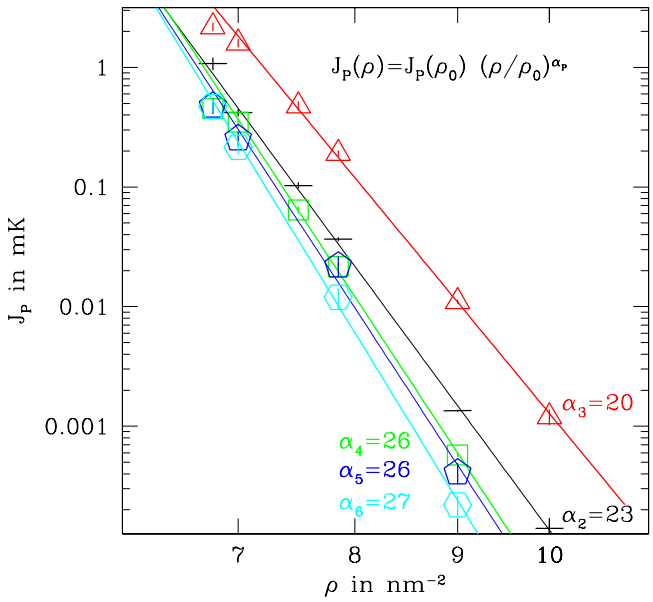

Figure 2. Helium-3 adsorbed on graphite: first-layer exchange frequencies versus the density.

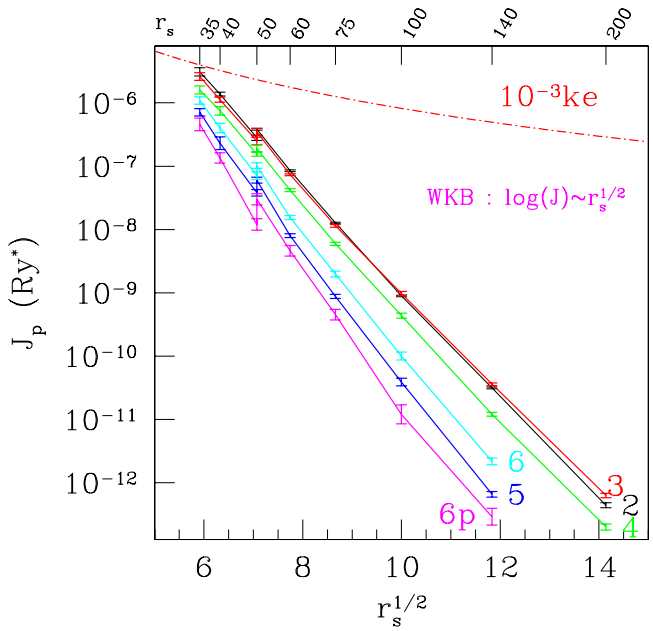

Figure 3. Exchange energies versus $r_s^{1/2}$. For $r_s \geqslant 50$, non-exchanging electrons are distinguishable, and for $r_s \leqslant 50$, the neighbouring electrons are spin polarized (preliminary results). One can see that near melting, exchange energies become comparable with the kinetic energy [8].

from exact diagonalizations on small periodic samples [12]. The number of parameters can be reduced by taking one of them to scale the energies. In addition, for spin-$\frac{1}{2}$, by using the identity $P_{ijk} + P_{ijk}^{-1} = P_{ij} + P_{jk} + P_{ki} - 1$, an effective pair exchange is defined which on the

triangular lattice reads $J_2^{\text{eff}} = J_2 - 2J_3$. Because J_2^{eff} can be positive or negative, J_4 is chosen to scale the energies.

The frustration of this Hamiltonian comes from two factors:

(i) geometrical frustration caused by the triangular lattice: even the simplest Heisenberg model is frustrated, but it has a Néel long-range order [13];
(ii) coupling competition: there are ferromagnetic coupling (the three- and five-body loops) and antiferromagnetic ones (the two-, four- and six-body loops).

A 'plane' in Hamiltonian space separates the phase diagram into a ferromagnetic region (large negative J_2^{eff} or large positive J_5) and an antiferromagnetic region (large positive J_2^{eff} or J_4 or J_6) (see figure 4). In agreement with WKB calculations in the strong-coupling limit, both helium and the Wigner crystal are ferromagnetic, since the three-particle exchange dominates. As shown on the phase diagram (figure 4), both the Wigner crystal and the second solid layer of helium-3 adsorbed on graphite become antiferromagnetic well before the melting transition. Instead of having a simple transition between two ordered states, as will be the case for the Heisenberg model (of equation (1)), the larger loops of four-body exchanges become important simultaneously when J_2 becomes of the same order of J_3. In the antiferromagnetic region, the point ($J_2^{\text{eff}}/J_4 = -2$, $J_5 = J_6 = 0$) presents a RVB-type ground state with a gap to all excitations. It is likely that most of this region of the phase diagram will be a single phase of spin liquid [12]. In the range of densities presented in figure 2, far from the melting transition, the first layer of helium-3 adsorbed on graphite is always ferromagnetic.

4. Approaching the melting transition

A remarkable feature is the similarity of the relative exchanges of the two solids when approaching the melting transition: the trajectories in the Hamiltonian space as a function of density (see figure 4) approach each other. Yet the interactions of these two systems are very different: a short-ranged strongly repulsive potential for helium and a long-ranged smooth potential for electrons. An underlying universal mechanism is suggested, possibly due to virtual vacancy–interstitial (VI) excitations [10]).

Here, we address the question of how the important exchanges depend on the density in the Wigner crystal. The figure 5 shows how the relative values of the Js change with density. At large r_s (small density or the strong-coupling limit), J_2^{eff} (in fact J_3) is the dominant exchange. Down to $r_s \sim 100$, the J_2–J_4 model is relevant and other exchanges are only weak perturbations. For smaller r_s, the five- and six-body exchanges start to play a role, as can be seen also in the phase diagram (figure 4).

At even smaller r_s, we see in figure 5 that all exchanges become of the same order of magnitude. Therefore, to limit the MSE Hamiltonian to loops of sizes two to six is questionable and we must look at larger loops. In addition, the importance of each type of exchange depends not only on the Js but also on the number of equivalent exchanges in the Hamiltonian. This number increases exponentially with the loop size n. The mean $\langle J_n \rangle$ and total $J_n^{(T)}$ exchange for loops of length n are defined by

$$\langle J_n \rangle = \frac{1}{n_T} \sum_{\text{shape}} n_{\text{shape}} J_n^{(\text{shape})}, \tag{5}$$

$$J_n^{(T)} = n_T \langle J_n \rangle, \tag{6}$$

where n_{shape} is the number of equivalent exchanges per site of a given shape and $n_T = \sum_{\text{shape}} n_{\text{shape}}$. As seen in figure 5, even if the hexagonal exchange is larger than the five-body exchange, the mean six-body exchange remains smaller.

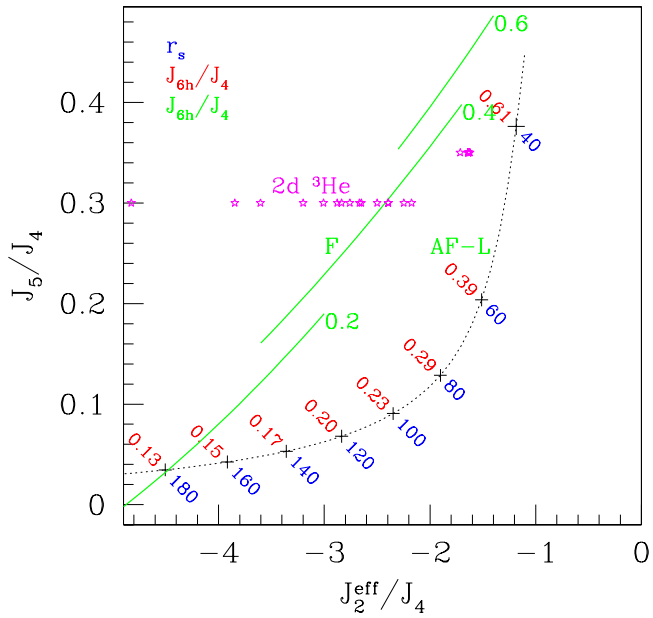

Figure 4. The zero-temperature magnetic phase diagram of the MSE Hamiltonian [12].

The importance of exchanges of length n can be measured by $J_n^{(T)}$. All the six- and seven-body exchanges have been calculated at $r_s = 40$ and 50. $\langle J_8 \rangle$ has been evaluated from a selection of 8 shapes amongst 17 possible eight-body shapes. At r_s larger than 75, we see that loops of length larger than 4 are indeed small perturbations. At $r_s = 50$, five- and six-body loops are no longer negligible and additional data are needed to judge the importance of even larger loops. At $r_s = 40$, we see that the exchanges of the largest loops lead to the most important contribution in the Hamiltonian.

The Curie–Weiss temperature θ is directly expressed in terms of $J_n^{(T)}$ as (note that $J_2^{(T)} = 3J_2$, $J_3^{(T)} = 4J_3$, $J_4^{(T)} = 6J_2$, $J_5^{(T)} = 12J_5$)

$$\theta = \sum_{n=2}^{n_{\max}} (-1)^n W_n J_n^{(T)} \qquad \text{with } W_n = -3\frac{n(n-1)}{2^{n-1}}. \tag{7}$$

Figure 6 shows the relative importance of loops of length n in this sum. At $r_s = 40$, convergence is clearly not reached.

A better way to look at the importance of various exchanges is via their contribution to the specific heat. At high temperature, the leading term of the MSE Hamiltonian can be written as

$$C_V \sim \frac{9}{4} N k_B \left(\frac{J_{C_V}}{T}\right)^2 \tag{8}$$

where $J_{C_V}^2$ is a positive quadratic form of the Js. J_{C_V} is used to scale temperatures and measure the typical energy associated with the spin correlations. Figure 7 shows the corrections of loops of size n to J_{C_V}. At the smallest r_s, even if the convergence is not clearly established, no divergence seems to occur. A divergence of J_{C_V} means a breakdown of the energy separation hypothesis needed in the Thouless theory. Interestingly, the breakdown appears when the melting transition takes place, leading naturally to the idea that the origin of the melting might be related to a divergence in the importance of very long loops of exchanges, perhaps caused by the unbinding of VI pairs.

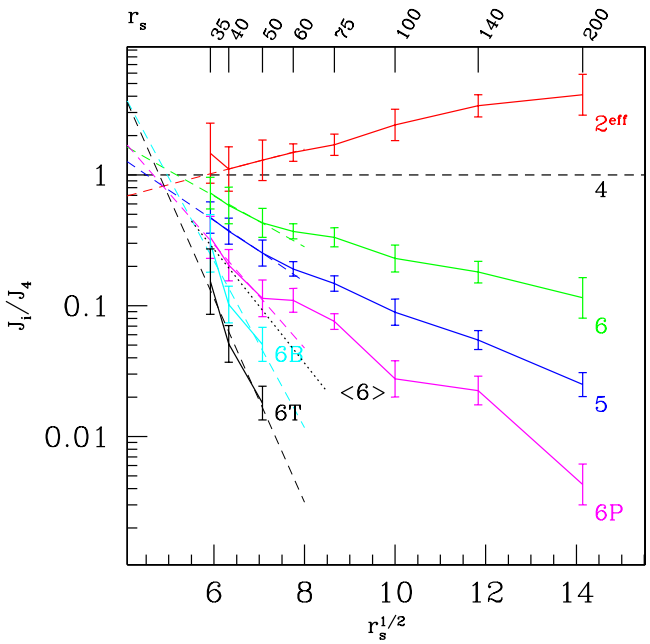

Figure 5. Relative exchange energies for the Wigner crystal versus $r_s^{1/2}$. The labels 6P, 6T, 6B stand for parallelogram, large triangle and the hexagonal shape where a site is replaced by the centre of the hexagon. Dashed lines are extrapolated guide lines. Note that all these values become of the same order of magnitude at smaller r_s. The dotted line represents the mean six-body exchange as defined by equation (5).

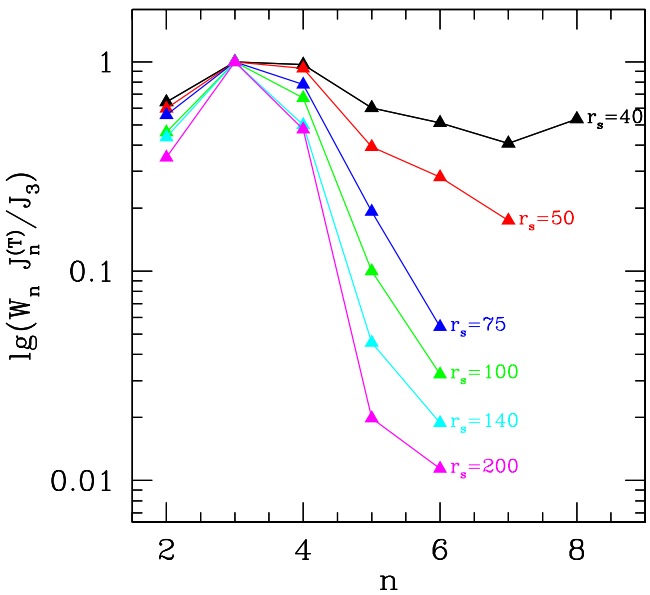

Figure 6. The importance of loops of length n (relative to J_3) to the Curie–Weiss temperature versus the length n of the loops for different r_s.

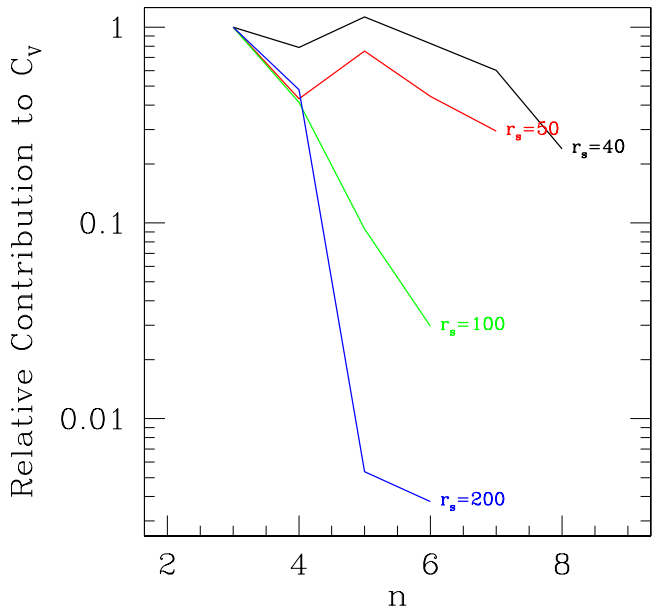

Figure 7. The importance of loops of length n (relative to J_2^{eff}) to the specific heat versus the length n of the loops for different r_s. The values correspond to the corrections due the loops of order n to J_{C_V} defined by equation (8) including loops up to order $n-1$.

5. Conclusions

For fermionic solids, PIMC allows one to evaluate exchange energies. These energies are then coupling parameters in a MSE Hamiltonian which can be studied by different techniques such as exact diagonalization. It is found that various two-dimensional systems have a dominant three-body exchange in the semi-classical limit (strong coupling) leading to a ferromagnetic ground state. As the quantum kinetic contributions increase, all exchanges become comparable with competitive ferromagnetic and antiferromagnetic interactions. Near melting it is found that the relative exchanges in the Wigner crystal are very similar to those obtained for a solid layer of helium-3 adsorbed on graphite, suggesting a possible universal behaviour of the exchange mechanism near the melting transition. Such mechanism could explain the importance of large-loop exchanges near the melting transition, even if no direct relation is yet proven.

Acknowledgment

Thanks are due to D S Greywall for the authorization to use one of his published figures [1].

References

[1] Greywall D S and Busch P A 1990 *Phys. Rev. Lett.* **65** 2788
Greywall D S 1990 *Phys. Rev.* B **41** 1842
[2] Roger M, Bauerle C, Bunke Yu M, Chen A-S and Godfrin H 1998 *Phys. Rev. Lett.* **80** 1308
[3] Thouless D J 1965 *Proc. Phys. Soc. London* **86** 893
[4] Bennett C H 1976 *J. Comput. Phys.* **22** 245
[5] Ceperley D M 1995 *Rev. Mod. Phys.* **67** 279
[6] Ceperley D M and Jacucci G 1987 *Phys. Rev. Lett.* **58** 1648

[7] Bernu B and Ceperley D 1999 *Quantum Monte Carlo Methods in Physics and Chemistry* ed M P Nightingale and C J Umrigar (Dordrecht: Kluwer)
[8] Bernu B, Candido L and Ceperley D 2001 *Phys. Rev. Lett.* **86** 870
[9] Roger M 1984 *Phys. Rev.* B **30** 6432
[10] Roger M, Hetherington J H and Delrieu J M 1983 *Rev. Mod. Phys.* **55** 1
[11] Voelker K and Chakravarty S 2001 *Preprint* cond-mat/0107151
[12] Misguich G, Bernu B, Lhuillier C and Waldtmann C 1998 *Phys. Rev. Lett.* **81** 1098
Misguich G, Bernu B, Lhuillier C and Waldtmann C 1999 *Phys. Rev.* B **60** 1064
[13] Bernu B, Lhuillier C and Pierre L 1992 *Phys. Rev. Lett.* **69** 2590